Single and Double Photoelectron Spectroscopy of Atomic Mercury†

John H. D. Eland* and Raimund Feifel

Oxford University, Physical and Theoretical Chemistry Laboratory, South Parks Road, Oxford OX1 3QZ, U.K.

David Edvardsson

Department of Quantum Chemistry, Uppsala University, Box 518, S-75120 Uppsala, Sweden

Received: May 5, 2004

Using the new time-of-flight photoelectron−photoelectron coincidence technique, we have recorded complete single and double photoelectron spectra of mercury at up to 48.4 eV photon energy. Many new satellite states of Hg^+ have been located both below and above the double ionization limits, and some have been identified with the aid of relativistic electronic structure calculations. The superexcited states autoionize to Hg^{2+} showing considerable channel specificity, apparently related most strongly to the atomic shell configurations of the final states. Direct double photoionization plays a relatively small part in the process of double ionization to the ground state of Hg^{2+}.

Introduction

The photoelectron spectrum of atomic mercury was first recorded in the energy range below 21 eV by Frost et al.,[1] who showed that ionization to the ground $^2S_{1/2}$ state is very weak relative to the formation of the $^2D_{5/2,3,2}$ levels of Hg^+. The earlier photoionization yield measurements of Brehm[2] and Berkowitz and Lifschitz[3] had already shown that formation of the ^2S state is dominated by autoionization from Rydberg levels converging on the ^2D states, and that strong continua start only at the convergence limits. This was elegantly confirmed by the variable wavelength photoelectron spectroscopy of Blake.[4] Photoelectron spectra taken at the He line wavelengths by Dehmer and Berkowitz,[5] Berkowitz et al.,[6] and Süzer et al.[7] then showed that the one-electron ionizations are accompanied by weak configuration interaction (CI) satellites corresponding to formation of the $5d^{10}6p$ configuration of Hg^+. This could be explained qualitatively at least by a substantial mixing of the excited configuration $5d^{10}6p^2$ in the ground state of the Hg atom. Later work on the photoionization of mercury concentrated on experimental measurement and theoretical evaluation of the partial cross sections and angular distributions for single electron photoionization from the different inner shells of the atom.[8−11] The use of relativistic theory was seen as essential.

The total cross-section for double photoionization of mercury over a range of photon energies is known from the work of Cairns et al.,[12] but the only previous spectroscopic investigation of the one-photon double ionization process is the low resolution work of Price and Eland.[13] In this paper we report complete, well-resolved photoelectron pair distributions from one-photon double ionization of mercury at 40.8 and 48.4 eV photon energies, obtained by a new technique, time-of-flight photoelectron−photoelectron coincidence (TOF−PEPECO). The single ionization photoelectron spectra recorded at the same time show new and detailed satellite structure below the double ionization limit, while the electron distributions in double photoionization reveal many new intermediate singly charged states embedded in the double ionization continua.

To interpret the spectra we have undertaken relativistic calculations on the electronic structure of mercury and its ions. The new calculations update and extend the pioneering calculations of Berkowitz and his colleagues.[5,6]

Experimental Section

The TOF−PEPECO technique[14] is based on the use of a pulsed vacuum−UV (VUV) lamp and a long (5.5 m) magnetic bottle time-of-flight electron spectrometer. Light pulses of 5−10 ns duration are produced at a repetition rate of 9 kHz by a capillary discharge in helium initiated by switching the stored charge of a capacitor, 150 pF at 10 kV, to the hollow-cathode electrode using a hydrogen thyratron. The operation of the lamp depends strongly on several factors including the gas pressure, repetition rate, gas purity, and mechanical design. The interplay of these factors is not yet fully understood, but details of the design will be published when development is completed. Individual atomic lines from the discharge are isolated by a grazing-incidence VUV monochromator and are refocused by a toroidal gold mirror into the source region of the magnetic bottle, where the light meets target molecules in an effusive jet from a 1 mm needle. Count rates of several hundred electrons per second are usual, implying a light intensity of the order of 10^6 photons per pulse at the point of use. The source end of the magnetic bottle is closed by the divergent field created by a NdFeB permanent magnet with a conically machined end; the field near the tip is about 0.4 T while in the ionization zone it is about 0.08 T. Electrons are guided along the 5.5m flight path by a solenoidal field of 10^{-3} T, shielded from the geomagnetic field by a layer of mumetal, to a chevron microchannel plate detector. Electron pulses are amplified, discriminated and registered by a time-to-digital converter card mounted in the personal computer monitoring the experiment. A critical feature is the provision of an *XYZ* translation stage upon which the permanent magnet is mounted, because the "tuning" of this position is found to be indispensable for good resolution. The

† Part of the special issue "Tomas Baer Festschrift".

* Corresponding author. E-mail: eland@physchem.ox.ac.uk.

10.1021/jp040332g CCC: $27.50
Published on Web 09/18/2004

electron energy resolution is strongly electron energy dependent; for energies below 2 eV lines 20 meV or narrower are seen, but by 10 eV the width is 100 meV and rises theoretically with the $^3/_2$ power of the energy. In practice, the resolution at high electron energy depends on the shape, as well as the width, of the light pulses. This effect can be compensated in one-electron photoelectron spectra as explained below, but not in the double ionization spectra.

Mercury vapor was produced from a small sample in a thermostatically controlled oven within the vacuum chamber, held at 100 °C. The vapor was condensed on a liquid nitrogen cooled surface opposite the tube leading from the oven.

Theoretical Methods

Multiconfigurational Dirac−Fock (MCDF) and relativistic configuration interaction (RCI) calculations were performed using the GraspVU set of programs.[15] This set of programs is a modification of the original GRASP92 program by Parpia et al.[16] In the MCDF method the atomic state wave functions are approximated by an expansion of *jj*-coupled configuration state functions (CSFs), where each CSF consists of linear combinations of Slater determinants. The configuration expansions of the wave functions were generated using the JJGEN program.[15] All radial wave functions are numerically represented on a logarithmic grid, and both wave functions and expansion coefficients are optimized to self-consistency. The energy functional constructed is optimized using the extended optimal level (EOL) scheme. A two-parameter isotropic nuclear model is used to represent the charge distribution of the nucleus. The value of the speed of light, *c*, used in all calculations is 137.0359895 au.

For all electronic states calculated, only the valence electrons were correlated by allowing single and double excitations into an active set of orbitals. For the neutral ground state the largest number of active orbitals consisted of the set {6s, 6p, 6d, 6f, 6g, ..., 9s, 9p, 9d, 9f, 9g}. Because of numerical instabilities in the MC−SCF procedure, full optimizations of all the orbitals were included only for the $n = 6$ shell. For higher n quantum numbers only orbitals of the outermost shell were optimized. In the singly and doubly charged atom, only the occupied valence orbitals were active.

Data Reduction

The conversion from electron time-of-flight (*TOF*) to energy *E* is effected by inversion of the simple relation

$$\mathrm{TOF} = t_0 + D/(E + E_0)^{1/2}$$

where D is the length of the flight path and t_0 and E_0 are constants for fixed experimental conditions. The energy offset may vary even during a single run, however, because of contact potential changes as the apparatus surfaces react to the target gas. Such changes, usually amounting to a few meV, are compensated by cross-correlation of blocks of data taken in time order.

As mentioned above, it follows from the flight time formula that the energy width of single peaks rises at high electron energy as the $^3/_2$ power of the energy, as the peak width in time remains a constant copy of the light pulse width. Unfortunately the light pulses are not simple peaks of Gaussian or any analytic form but often have asymmetric tails and weak subsidiary peaks, mainly on the forward (early) side. These defects have negligible effect on double ionization spectra where the electron energies are low, but severely distort single ionization spectra at the short wavelengths. We have used a deconvolution procedure to diminish their effects on the photoelectron spectra taken at 40.8 and 48.4 eV photon energy. The procedure is based on Siska's iterative method[17] and is applied in the time domain before conversion to energy. The light pulse shape is determined in separate experiments.

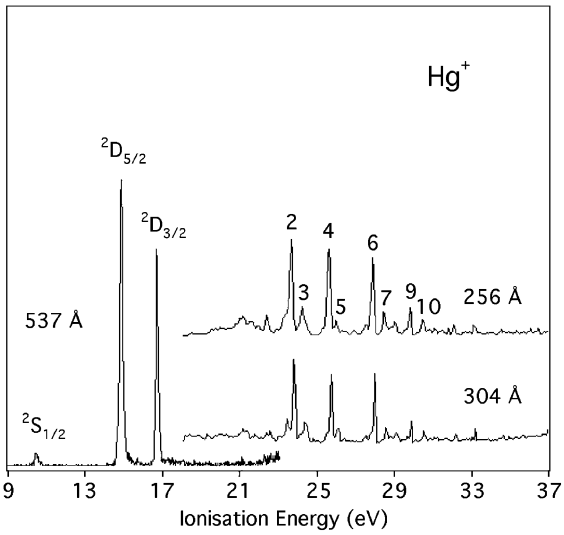

Figure 1. Photoelectron spectra for single ionization of mercury at three wavelengths, as indicated. The spectra at the two shortest wavelengths are deconvoluted versions of the raw data, as explained in the text.

TABLE 1: Major Satellite Peaks in the Photoelectron Spectrum of Hg^+ at Both 40.8 and 48.4 eV Photon Energy

peak	energy (eV) ± 0.05 eV	height $Hg^+(^2D_{5/2}) = 2000$	state	exptl energy	theor rel energy
1	22.4	5			
2	23.64	40	$5d^9(5/2)6p^2(^3P_0)$	0.0	0.0
3	24.24	10			
4	25.60	35	$5d^9(3/2)6p^2(^3P_0)$	1.96	2.38
5	25.96	5			
6	27.87	35	$5d^9(5/2)6p^2(^1S_0)$	4.23	4.38
7	28.48	7			
8	29.00	4			
9[a]	29.78	10	$5d^9(3/2)6p^2(^1S_0)$	6.14	6.28
10[a]	30.46	5			
12[a]	33.13	4			

[a] These peaks appear strongly in double ionization, Table 3, and their full intensities are not seen in the single electron photoelectron spectrum.

Experimental Results

Figure 1 shows single electron photoelectron spectra from runs at three wavelengths, corresponding to photon energies of 23.08, 40.81, and 48.37 eV. The low binding energy part looks exactly the same at all wavelengths and is displayed only once, as it contains no new information. New features are seen in the high energy region between 18 and 37 eV binding energy and match well in the independent data at the two wavelengths. There are other features at higher apparent binding energy, but they are due to double ionization and many remain fixed in electron energy, like Auger lines, not in binding energy. They are seen much more clearly in the electron pair data, presented below. The energies and approximate intensities of the main satellite peaks in the single electron spectra are collected in Table 1.

The double ionization data are essentially two-dimensional, and one example of a full double ionization map is given as

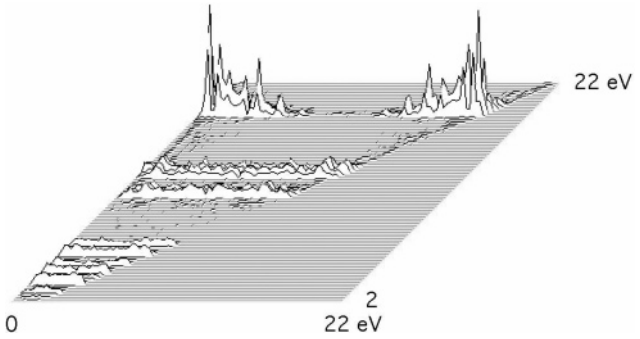

Figure 2. Isometric projection of the full two-dimensional double photoelectron spectrum of mercury at 48.4 eV photon energy. The intensity is shown as a function of the sum of the two electron energies (into the page) and the energy of either electron (across the page). Each final state of Hg^{2+} produces a line of signals, with peaks showing autoionization, the whole distribution being symmetrical at about half the maximum electron energy. The low resolution of this figure smears out the fine detail, which is shown in the following projections.

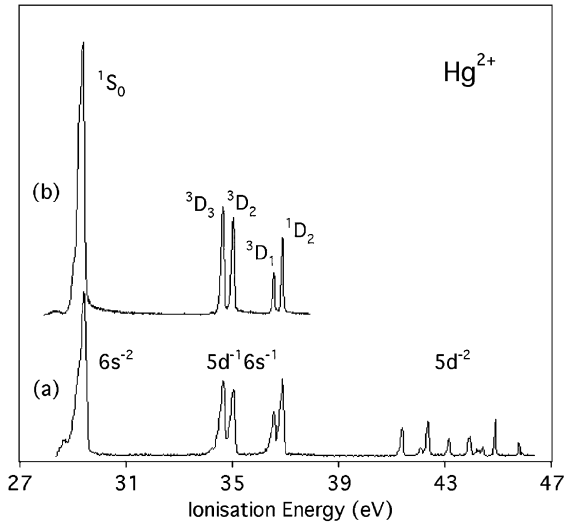

Figure 3. Double photoelectron spectra of mercury at 40.8 and 48.4 eV photon energy, showing the populated states of Hg^{2+}.

Figure 2. The information can be presented more clearly as one-dimensional projections of the full maps, of which the simplest are spectra of the doubly charged ions shown in Figures 3 and 4. All the states of Hg^{2+} visible in the spectra can be identified from the results of optical spectroscopy;[18] new information is provided by their intensities in photoionization, listed in Table 2. The hole states in the table have been labeled using LS coupling nomenclature, even though the coupling may be nearer $J-J$ or intermediate type. Because the peak at 42.34 eV (attributed to $J = 2$) is considerably stronger than the one at 43.11 eV (attributed to $J = 3$), we originally considered whether to exchange the J values given in Moore's tables.[18] This question arises from the usual rule that relative photoionization intensities of lines from a single configuration are generally close to the ratios of statistical weights, when allowance has been made for well-known effects such as the variation of cross section with excess energy. Here, the rule holds better for the $5d^96s$ configuration of Hg^{2+} than for the $5d^86s^2$ configuration, where there are some intensity anomalies including the one noted above. In fact our electronic structure calculations completely confirm the spectroscopic order; the inversion of $J = 2$ and $J = 3$ is due to strong configuration mixing.

In addition to the spectrum of the doubly charged atom, the photoionization maps contain the spectra of electrons whose

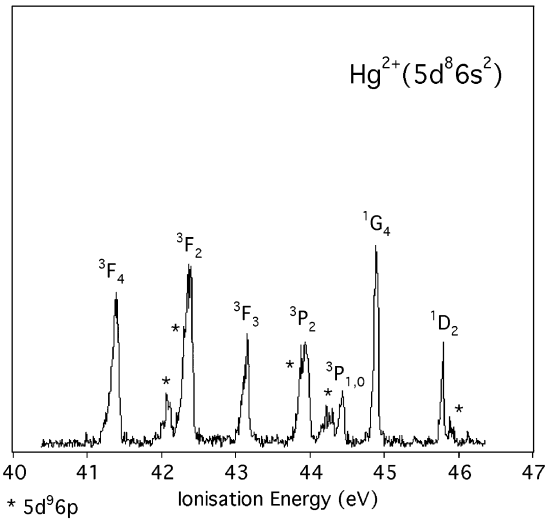

Figure 4. Detail of the states of Hg^{2+} formed in 48.4 eV photoionization predominantly by $5d^{-2}$ ionization. Asterisks indicate states arising from the configuration $5d^96p$.

TABLE 2: Partial Cross Sections (Mb) for Double Photoionization to the States of Hg^{2+} below 48 eV[a]

energy (eV)[15] and state	σ(304 Å) (Mb)	σ(256 Å) (Mb)
29.19 $5d^{10}...{}^1S_0$	2.61	2.16
34.51 $5d^96s...{}^3D_3$	0.54	0.68
34.90 $5d^96s...{}^3D_2$	0.47	0.51
36.43 $5d^96s...{}^3D_1$	0.14	0.28
36.77 $5d^96s...{}^1D_2$	0.25	0.50
41.33 $5d^86s^2...{}^3F_4$		0.13
42.01 $5d^96p$		0.04
42.34 $5d^86s^2...{}^3F_2$		0.17
43.11 $5d^86s^2...{}^3F_3$		0.07
43.90 $5d^96p$ blend		0.04
43.94 $5d^86s^2...{}^3P_2$		0.07
44.20 $5d^96p$ blend		0.07
44.40 $5d^86s^2...{}^3P_{1,0}$		0.07
44.87 $5d^86s^2...{}^1G_4$		0.10
45.77 $5d^86s^2...{}^1D_2$		0.04
45.93 $5d^96p$ blend		0.01

[a] Experimental relative intensities have been normalized to overall double photoionization cross sections of 4 Mb at 304 Å and 5 Mb at 256 Å from Cairns et al.[12]

emission leads to each final state of Hg^{2+}. All events populating a given final state produce electron pairs with the same energy sum, $E_1 + E_2$, and form a distribution symmetrical about the central energy $(E_1 + E_2)/2$, as seen in Figure 2. The distributions of the energies E_1, shown in Figures 5−7, contain many sharp lines from autoionization of intermediate superexcited states of Hg^+, with the characteristic that the lower of the two electron energies is independent of the ionizing photon energy. This independence is demonstrated for the case of ionization to $Hg^{2+}(^1S_0)$ in Figure 5. Because the resolution is better in our apparatus for low energy electrons we display the low energy electron distributions on ionization energy scales (equivalent to taking the higher electron energy from the photon energy) in Figures 6 and 7. Some autoionizing lines appear as precursors for several final dication states, while others are specific to a single final state. The energies and branching proclivities of some of the prominent autoionizing states of Hg^+ are listed in Table 3.

Theoretical Results and Discussion

Identities of the Highly Excited States of Hg^+. The first excited states of Hg^+ are the two $5d^{-1}$ single hole states. As a

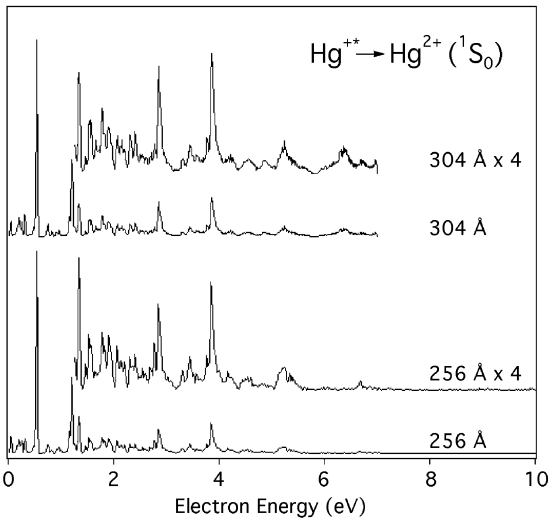

Figure 5. Spectra showing the distribution of photoelectron energies leading to formation of the Hg^{2+} ground state, $^1S_0$, at two wavelengths. The peaks which remain fixed in electron energy are the "Auger" lines from autoionization via intermediate states of superexcited Hg^+.

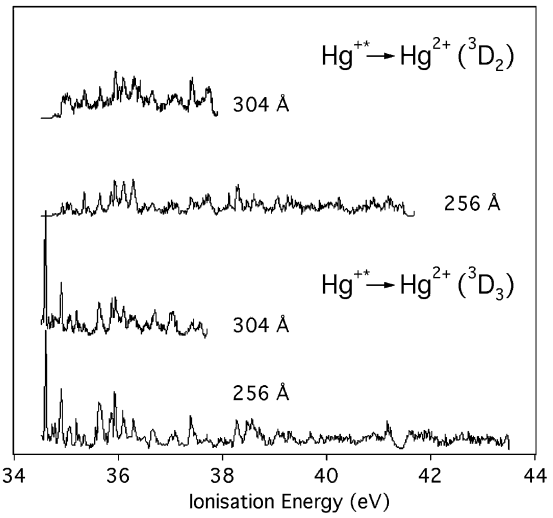

Figure 6. Photoelectron energy distributions in formation of two of the states from $5d^{-1}6s^{-1}$ ionization, shown on a scale of ionization energy. Here the peaks give the energies of the "photoelectron" lines in each autoionization process.

check on the theoretical method we have calculated their energies relative to the ground state, and find 4.49 eV ($^2D_{5/2}$) and 6.34 eV ($^2D_{3/2}$) in excellent agreement with the experimental 4.40 and 6.27 eV. Higher excited states of Hg^+ both below and above the double ionization thresholds may be either Rydberg states belonging to series converging on higher Hg^{2+} levels, or may arise from multiply excited configurations. According to the calculations of Berkowitz et al.,[3,5,6] the ground state of the atom can be described as a strongly mixed configuration including much $5d^{10}6p^2$ as a leading term. From the new calculation we obtain a more detailed description of the ground state as

$$0.9847\,(5d^{10}6s^2) + 0.1265\,(5d^{10}6p^2) + 0.1129\,(5d^{10}6p'^2) - 0.0303\,(5d^{10}7s^2) - 0.0129\,(5d^{10}6d^2)$$

Here p′ represents the $p_{1/2}$ and p represents the $p_{3/2}$ subshells, respectively.

The doubly excited configurations might be expected to lead to ionization populating $5d^96p^2$ and similar three-hole−two-particle states of the ion. This idea is confirmed by the appearance in the spectra of pairs of peaks of comparable intensity with a separation near 2 eV, characteristic of the $^5/_2$−$^3/_2$ splitting of the d^9 term. Examples are the peaks numbered 2 and 4, 3 and 5, 6 and 9, and 7 and 10 in Figure 1. Contrary to the observation of autoionizing superexcited states of rare gas ions,[19] there are no evident converging Rydberg series to be seen. To identify the most prominent peaks, we have first examined the known states of the related atoms Pb^I and Tl^{II}.[18] The comparison suggested, and the detailed calculations confirm that peaks 2, 4, 6, and 9 all arise from the leading configuration $5d^96p^2$. The observed and calculated relative energies are listed in Table 1. We have not yet calculated the full spectrum of Hg^+, but this may be the object for future work.

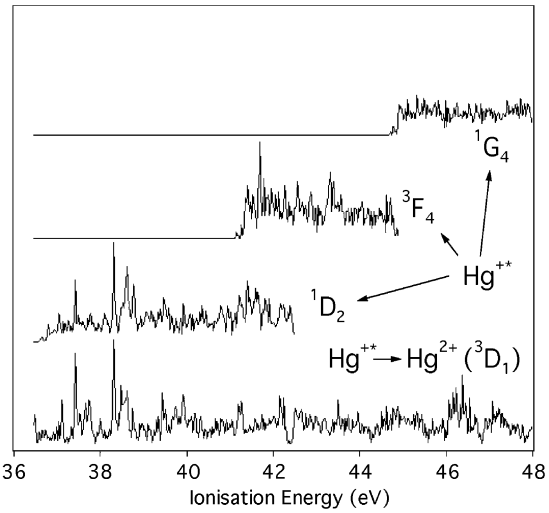

Figure 7. Photoelectron energy distributions in formation of the two higher $5d^{-1}6s^{-1}$ states and of two $5d^{-2}$ states of Hg^{2+}, again on an ionization energy scale as in Figure 6. The lack of peaks on the distribution for $^1G_4$ formation suggests a mainly direct process in this case.

TABLE 3: Prominent Autoionizing States of Hg^+

peak no.[a]	energy (eV) ± 0.05 eV	intens	Hg^{2+} state formed
9	29.73	3662	$^1S_0$
10	30.39	2147	$^1S_0$
11	30.53	923	$^1S_0$
12	32.05	887	$^1S_0$
13	33.06	1292	$^1S_0$
14	34.45	980	$^1S_0$, broad
15	34.58	309	$^3D_3$
16	34.89	243	$^3D_3$, ($^3D_2$)
17	35.64	409	$^3D_3$, $^3D_2$ broad
18	35.85	203 + 77	$^1S_0$,$^3D_3$, $^3D_2$
19	35.93	223	$^3D_3$, $^3D_2$
20	36.10	222	$^3D_3$, $^3D_2$
21	36.29	170	$^3D_3$, $^3D_2$
22	37.40	91 + 144	$^3D_3$, $^3D_2$,$^3D_1$,$^1D_2$
23	38.28	218 + 174	$^3D_3$, $^3D_2$,$^3D_1$,$^1D_2$
24	41.23	131	$^3D_3$, $^3D_1$, ($^1D_2$?)
25	41.69	31	$^3F_4$
26	43.32	63	$^3F_4$

[a] Numbering continues from Table 1.

Branching in Autoionization. As in the rare gases,[19] the superexcited states of Hg^+ show specificity in their autoionization to different final states of Hg^{2+}. The states which on emission form Hg^{2+} in states of the $5d^96s$ configuration populate all energetically possible ^3D or ^1D states, but, with one exception, do not populate the accessible $^1S_0$ state at all. The one exception is the line numbered 18 in Table 3, which is also

somewhat wider than nearby levels. Similarly, the rather few distinct lines seen to populate Hg^{2+} states of the $5d^8 6s^2$ configuration do not go to either $5d^9 6s$ states or to $^1S_0$. These observations suggest that the autoionization process tends to conserve some element of the electron configuration, perhaps specifically the 5d occupancy.

Intensities of the Dicationic States. The final states of Hg^{2+} are certainly populated by both indirect and direct photoionization. In view of this, it is rather surprising that the relative intensities of the different states from each configuration accord fairly well with their relative statistical weights. The relative intensities of the different configurations are even more surprising; whereas $6s^{-1}$ ionization has a negligible probability in direct single ionization, $6s^{-2}$ double ionization has by far the largest cross section per available electron. The raw relative cross sections for $6s^{-2}$, $5d^{-1}6s^{-1}$, and $5d^{-2}$ ionizations at 48.4 eV photon energy are 5:4.5:1, but when energy effects are allowed for assuming a linear cross-section law they become nearly equal (2:3:3).

Extent of Direct and Indirect Photoionization Processes. Unlike in single ionization, indirect double ionization happens at all photon energies and can be disentangled from the direct process only by analysis of well-resolved electron energy distributions. The distributions shown for Hg in Figures 5−7 emphasize peaks on weak apparent continua, except for the $5d^{-2}$ ionizations, which may be mostly direct. Resolution limitations mean that we cannot entirely exclude the idea that the apparent continua may themselves be conflations of unresolved lines. If our spectra are taken at face value, however, photoionization to Hg^{2+} ($^1S_0$) is 35% direct and 65% indirect at 48.4 eV photon energy, and even more indirect at the lower photon energy.

Conclusions

We have measured complete double photoionization spectra of mercury at 40.81 and 48.37 eV photon energy and found a great wealth of autoionization structure. The spectrum of Hg^+, determined simultaneously, also contains many new peaks, some of which represent states based on configurations important in the description of ground state mercury atoms. Further theoretical work is needed, particularly to explore the importance of initial state correlation in determining the Hg^+ spectrum.

Acknowledgment. D.E. would like to thank Per Jönsson at the Malmö University for providing the GraspVU program. R.F. thanks the Swedish Research Council (VR) and the Swedish Foundation for International Cooperation in Research and Higher Education (STINT) for financial support of his stay at Oxford University. We acknowledge financial support from the EPSRC.

References and Notes

(1) Frost, D. C.; McDowell, C. A.; Vroom, D. A. *Chem. Phys. Lett.* **1967**, *1*, 93.
(2) Brehm, B, *Z. Naturforsch.* **1966**, *21a*, 196.
(3) Berkowitz, J.; Lifschitz, C. *J. Phys. B* **1968**, *1*, 438.
(4) Blake, A. J. *Proc. R. Soc. London*, **1971**, *A325*, 555.
(5) Dehmer, J. L.; Berkowitz, J. *Phys. Rev.* **1974**, *A10*, 484.
(6) Berkowitz, J.; Dehmer, J. L.; Kim, Y. −K.; Desclaux, J. P. *J. Chem. Phys.* **1974**, *61*, 2556.
(7) Süzer, S.; Lee, S.-T.; Shirley, D. A. *Phys. Rev.* **1976**, *A13*, 1842.
(8) Kobrin, P. H.; Heiman, P. A.; Kerkhoff, H. G.; Lindle, D. W.; Truesdale, C. M.; Ferrett, T. A.; Becker, U.; Shirley, D. A. *Phys. Rev.* **1983**, *A27*, 3031.
(9) McQuaide, B. H.; Banna, M. S.; Gerard, P.; Krause, M. O. *Phys. Rev.* **1987**, *A35*, 1603.
(10) Svensson, S.; Stranges, S.; Adam, M. Y. *Phys. Rev.* **1993**, *A48*, 3051.
(11) Kutzner, M.; Tidwell, C.; Vance, S. E.; Radoyevi×c4, V. *Phys. Rev.* **1994**, *A49*, 300.
(12) Cairns, R. B.; Harrison, H.; Schoen, R. I. *J. Chem. Phys.* **1970**, *53*, 96.
(13) Price, S. D.; Eland, J. H. D. *J. Phys., B: At. Mol. Opt. Phys.* **1990**, *23*, 2269.
(14) Eland, J. H. D.; Ho, S.S. W.; Worthington, H. L. *Chem. Phys.* **2003**, *290*, 27.
(15) Jönsson, P. Private communication.
(16) Parpia, F. A.; Froese Fischer, C.; Grant, I. P. *Comput. Phys. Commun.* **1996**, *94*, 249.
(17) Siska, P. E. *J. Chem. Phys.* **1973**, *59*, 6052.
(18) Moore, C. E. *Circ. Natl. Bur. Stand. US* 497 1958.
(19) Eland, J. H. D.; Vieuxmaire, O.; Kinugawa, T.; Lablanquie, P.; Hall, R. I.; Penent, F. *Phys. Rev. Lett.* **2003**, *90*, 053003.